Horizontal Phase-Space Distortions Arising from Magnetic Pulse Compression of an Intense, Relativistic Electron Beam

S. G. Anderson, J. B. Rosenzweig, P. Musumeci, and M. C. Thompson
Department of Physics and Astronomy, UCLA, 405 Hilgard Avenue, Los Angeles, California 90095, USA
(Received 21 June 2002; published 14 August 2003)

We report detailed measurements of the transverse phase space distortions induced by magnetic chicane compression of a high brightness, relativistic electron beam to subpicosecond length. A strong bifurcation in the phase space is observed when the beam is strongly compressed. This effect is analyzed using several computational models and is correlated to the folding of longitudinal phase space. The impact of these results on current research in collective beam effects in bending systems and implications for future short wavelength free-electron lasers and linear colliders are discussed.

DOI: 10.1103/PhysRevLett.91.074803 PACS numbers: 29.27.Bd, 41.60.Ap, 52.59.Sa

Future high energy physics accelerators [1,2] and fourth-generation light sources [3] will require subpicosecond rms electron pulses, or bunches. In addition, these applications demand the brightest beams possible. However, the length of beams produced in the highest brightness electron sources, rf photoinjectors, has a lower limit of several picoseconds. This limit is not due to restrictions on the lasers used to create the beams, but rather to large internal space-charge forces. The method used to minimize the transverse emittance after acceleration and transport of space-charge dominated [4] beams, termed emittance compensation [5,6], determines the beam density required to balance transverse space-charge and external focusing forces. As longitudinal focusing is not as effective as transverse focusing in the photoinjector, debunching results, and the bunch lengths resulting from this process make compression of the beam after the injector necessary for advanced applications [2].

The most common method of pulse compression uses a magnetic chicane [7], which when combined with off-crest acceleration in the radio-frequency (rf) linear accelerator (linac) used to boost the beam energy U allows rearrangement of the electrons' longitudinal position $\zeta = z - v_b t$, where v_b is the nominal beam velocity. As the path lengths of highest momenta p electrons are shortest, a negative (ζ, p) correlation leads to longitudinal compression. This process comes at a price, however, in that collective fields may severely distort the horizontal (x, bend plane) phase space. This distortion arises directly through transverse forces, or indirectly when a longitudinal force changes the electron energy during bending, giving rise to a subsequent trajectory error. For ultrarelativistic ($\gamma = U/m_e c^2 \gg 1$, $v \simeq c$) electrons, the energy changes induced during the motion are expected to arise mainly from coherent synchrotron radiation (CSR). These energy changes may be so pronounced that a newly predicted microbunching instability develops [8].

Previous studies of collective effects during the chicane compression process have been carried out where transverse emittance growth and changes in the momentum spectrum [9,10] were observed in the compressed beam. These studies were performed in the 40–60 MeV energy range, and the observed emittances and momentum spectra were compared to predictions from the simulation code TRAFIC4 [11]. From this comparison, evidence for strong CSR emission was deduced, with the implication that significant effects in the experiments were due to acceleration fields. Other measurements of magnetic compression have been performed with higher energy beams at Argonne National Laboratory, Deutsches Elektron Synchrotron, and Brookhaven National Laboratory [12], with CSR again playing a significant role in causing the observed emittance growth and longitudinal phase space distortions. It is notable that modeling of these experiments, which have concentrated on longitudinal phase space characteristics, has not reproduced some of the most striking aspects of the data, such as the severity of the beam's momentum spectrum modulation.

While these previous measurements have allowed tests of collective effects in high brightness beam compression, the distortion of the transverse phase space has been quantified only through examination of the rms normalized emittance, $\varepsilon_{n,x} = \beta\gamma\sqrt{\langle x^2\rangle\langle x'^2\rangle - \langle xx'\rangle^2}$, where $\beta\gamma = p/m_e c$ is the average normalized beam momentum. In the experiments reported here, the beam's horizontal phase space is directly sampled, allowing an accurate, shot-by-shot phase space reconstruction. These reconstructions give an unprecedented view of the collective transverse beam dynamics during compression, revealing a filamentary structure reminiscent of the strongly modulated longitudinal phase space in experiments mentioned above. Further, these measurements were performed with a lower beam energy (below 12 MeV), and thus explore a regime where velocity fields (i.e., space charge) play a dominant role. Such lower energy compression may be needed for applications such as Thomson scattering production of subpicosecond x-ray pulses [13] which demand moderate (20–50 MeV) final energies.

The measurements presented here were performed using the rf photoinjector in the UCLA Neptune Advanced Accelerator Laboratory [14]. The photoinjector beam is created using a 1.6 cell rf photocathode gun [15]. The 0.25 nC, 4 MeV beam produced by the gun is then emittance compensated and accelerated further with a plane wave transformer (PWT) linac [16]. The beam exits the PWT with $U \simeq 12$ MeV; the remainder of the photoinjector consists of the compressor and various beam diagnostics. The gun and PWT are independently phased, allowing use of the PWT to impart the proper (ζ, p) correlation for compression.

The electron bunch is compressed using a compact chicane magnet system [14]. The compressor has $R_{56} = \partial(\delta\zeta)/\partial(\delta p/p) = 3.5$ cm (in TRANSPORT [17] notation) at the design 22.5° bend angle, which optimally compresses the beam when injected into the PWT at roughly $\theta = \tan^{-1}\lambda_{\rm rf}/2\pi R_{56} = 25°$ ahead of the peak accelerating phase in the $\lambda_{\rm rf} = 10.5$ cm structure. Horizontally (bend plane) focusing magnet edge angles are included at the entrance and exit of the chicane, to avoid excessive vertical focusing that would otherwise cause the beam to focus sharply inside of the fourth magnet, giving an overly dense beam during compression.

Since the inner and outer sets of magnets in the chicane are identical pairs, the residual dispersion $\eta_x = \partial x/\partial(\delta p/p)$ was minimized experimentally by using trim coils in the inner set to eliminate the beam horizontal centroid variation with U at a detection screen downstream of the chicane exit. The calculated normalized rms emittance growth attributable to the measured residual η_x is negligibly small, below 10^{-7} m rad.

In order to study the beam's horizontal phase space (x, x') evolution for differing degrees of compression, an array of diagnostics were used to determine the beam's longitudinal and transverse characteristics. The rms bunch length (σ_z) diagnostic employed is a polarizing Michelson interferometer which analyzes coherent transition radiation [18] emitted from the electron beam's impact on a metal foil [19].

The transverse phase space is measured using a slit-based system [20–22], in which the beam is collimated by a slit mask into narrow beamlets, allowing single-shot the reconstruction of the original beam phase space and determination of $\varepsilon_{n,x}$. Specifically, the horizontal distribution p_x of each beamlet combined with the slit geometry and drift distance from the slits to the detecting screen gives the p_x distribution at the position of the beamlet. This method takes the projection of the beamlets onto the x axis and therefore averages over variations in y. These variations are always present in photoinjector beams because the effects of radial space charge produce a beam distribution which is not separable in Cartesian coordinates. Also, since this technique samples the p_x distribution at a finite set of x positions, to aid in visualization the presented trace space (related to phase space by $x' = p_x/p$) plots are derived by interpolation from one slit position to the next. The inherent resolution of the total $\varepsilon_{n,x}$ measurement, is 0.5 mm mrad for our experimental scenario, with a minimum angular resolution of 25 μrad, and a (single-slit) rms phase space area resolution of 0.1 mm mrad. Detailed descriptions of slit-based phase space diagnostics are given in Refs. [21,22]. The vertical emittance $\varepsilon_{n,y}$ was measured by the quad scanning technique; no significant growth in $\varepsilon_{n,y}$ was observed when the beam was compressed.

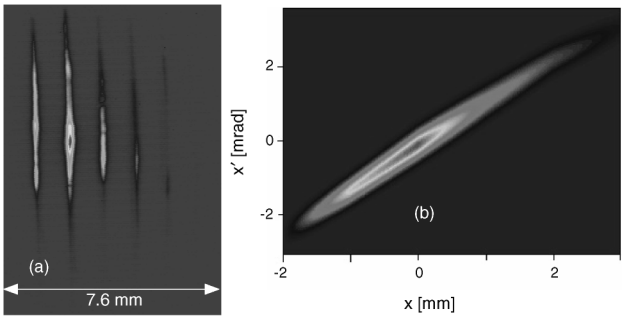

FIG. 1. (a) Image of an uncompressed beam passing through the slit mask. (b) Trace space derived from the image in (a).

In order to evaluate the effects of compression on the horizontal phase space, we first determined the bunch length. Here σ_z was measured at various PWT phases and chicane magnet settings. It was found to vary between 4 ps uncompressed and 0.6 ps at full compression, in agreement with both linear transport models and TREDI [23] simulations. The agreement between measured σ_z and simulation indicates that the compression system functioned as expected and provides a benchmark for parameters such as PWT phase and beam energy.

The slit system was then employed to measure the horizontal phase space distribution and rms emittance of the beam as a function of σ_z. This was accomplished by setting the bend angle to 22.5° and varying the PWT phase. Measurements holding the PWT phase constant and varying the chicane's R_{56} gave similar results.

Figure 1 shows a post-slit beam image, and the associated phase space reconstruction, for a beam that does not compress in the chicane (when the PWT phase is set to minimize energy spread). In Fig. 2 the PWT phase has been set to maximally compress the beam. Here the slit

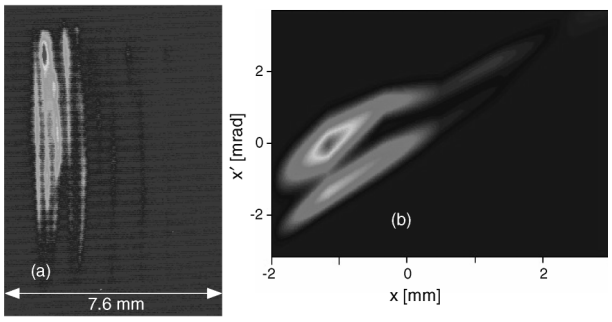

FIG. 2. (a) Image of a compressed beam passing through the slit mask. (b) Trace space derived from the image in (a).

image shows that the beamlets clearly split into separate components. This splitting indicates that the phase space of the compressed beam is bifurcated, as shown in the phase space plot [Fig. 2(b)]. In other words, distinct parts of a beamlet have the same slit position but differing mean angle, producing a split image at the screen. The observed splitting increased as σ_z was decreased and depended on vertical position within the beamlet; it was greatest in the vertical center of the beam, where the transverse space-charge forces are maximized.

Slit images such as those in Figs. 1 and 2 were recorded for differing PWT phase and $\varepsilon_{n,x}$ was calculated from those images. The result is given in Fig. 3. The plot shows that $\varepsilon_{n,x}$ increases from an uncompressed value of 6 mm mrad to about 20 mm mrad at full compression. We note also a sharp change in $\varepsilon_{n,x}$ at a PWT phase of 72°, the point where the onset of phase space bifurcation is observed.

The phase space bifurcation shown in Fig. 2 was a consistent feature of the data collected. The severity of this effect, as measured by the emittance growth $\Delta\varepsilon_{n,x}$, is strongly dependent on the degree of compression (Fig. 3). In addition, it was found to be sensitive to the horizontal beam size at the entrance of the chicane $\sigma_{x,0}$, with $\Delta\varepsilon_{n,x} = 4$ mm mrad for $\sigma_{x,0} = 2.2$ mm, while for $\sigma_{x,0} = 1.1$ mm, $\Delta\varepsilon_{n,x} = 24$ mm mrad was observed. For $\sigma_{x,0} = 2.2$ mm, the bifurcation was nearly eliminated.

We employed several different computer codes, which use different physical models, to simulate the compression process and gain information about the sources of the observed effects. First, PARMELA [24] was employed, both to provide input phase space distributions to other codes and to run through the chicane magnets using the 3D point-by-point space-charge calculation. This calculation uses a quasistatic approximation, which means that the effects of acceleration fields [25] are *not* included in the physics model.

TREDI, a tracking code that computes self-consistent, retarded Lienard-Wiechart potentials to yield the collective beam fields, was also used to simulate the compression process. As such, TREDI implicitly accounts for both the velocity and acceleration fields in the problem. Both TREDI and 3D PARMELA are computationally intensive, and thus 2500 simulation particles were used.

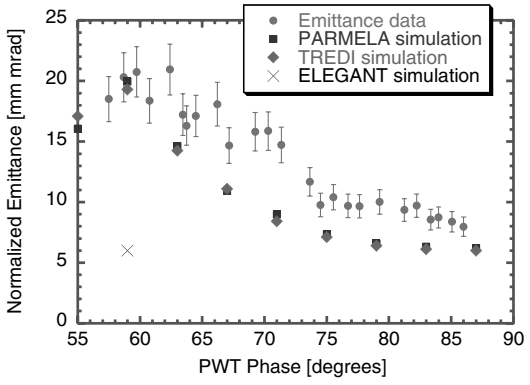

FIG. 3. Normalized horizontal emittance as a function of PWT injection phase.

Results of these simulations are given in Fig. 3; they indicate that velocity field space-charge forces contribute most of the observed $\Delta\varepsilon_{n,x}$, as the TREDI results closely agree with those from PARMELA, and both follow the experimental results. The PARMELA distributions were also used as input to ELEGANT [26], to calculate $\Delta\varepsilon_{n,x}$ due to CSR alone. The ELEGANT results indicate that CSR effects did not contribute to the $\Delta\varepsilon_{n,x}$ simulated with TREDI. While the PARMELA/TREDI results give agreement with the emittance data at both weak compression and full compression, the threshold effect of rapid emittance growth near the PWT phase of 72° is not reproduced by simulation. In the simulations, the associated (x, x') distribution bifurcation is also notably weaker.

We now note some relevant properties of the particle simulations used. The first is that PARMELA and TREDI employ relatively few simulation particles N_s to resolve effects which involve correlations throughout the beam's full 6D phase space. Use of small N_s also leads to numerical Coulomb heating and loss of coherent phase space structures. Thus, although we expect the calculations to approximate rms quantities such as $\varepsilon_{n,x}$ well, microscopic phase space details may not be reproduced.

To avoid the problems of particle-based calculations, and gain insight into the role of space charge in this system, we employed a model simulation based on beam slices. In this model we break the bunch up into longitudinal slices (in z) and track the evolution of each slice's centroid and rms envelope. Each ζ slice is modeled as a uniform ellipsoid of charge of some initial momentum offset and zero momentum spread. Space-charge forces, in the quasistatic approximation, are calculated to give the slice-to-slice centroid force; the gradient of these forces is also used to calculate the focusing effects of the slices on each other. These focal forces, as well as the slices' self-forces, are implemented in rms envelope equations. The details of this calculation are provided in Ref. [22].

In the absence of collective forces, the configuration space of centroids (x, ζ) shows the slices forming a "U" shape that folds down into a line in x as the beam traverses the final chicane dipole, where the relative slice positions in ζ do not change much. The impact space charge has on this folding beam can be understood qualitatively; as the two (high- and low-momentum) components of the beam are forced together they repel, and at the exit of the compressor these components have distinct central values of p_x. Space-charge repulsion during the folding has a maximum value roughly proportional to $\sigma_{x,0}^{-1}$, thus providing a simple explanation of the observed dependence of $\Delta\varepsilon_{n,x}$ on $\sigma_{x,0}$. Further, in our model, the bifurcation of the (x, x') space is enhanced by the gradient in the forces due to nearby slices; their repulsion falls

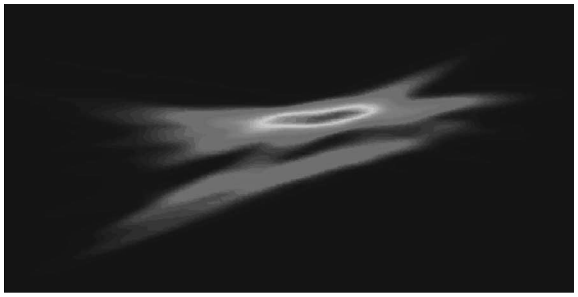

FIG. 4. Contour plot of the horizontal trace space produced by the slice model simulation after the compressor.

with distance, and when the slice ellipsoids are disjoint, they serve to focus each other to produce a smaller σ_x.

Initial conditions for the slice simulations were obtained by use of rms information from PARMELA. The results of the slice simulations produce more notable phase space bifurcations (generated from the combination of the simulated horizontal centroid and ellipsoid dimensions) than those obtained from particle codes. Even so, the phase space features, as shown in Fig. 4, are not as intricate as in the measurements. This is partly due to limitation of the forces in our model to only linear variations over a beam slices, whereas the repulsive forces in the experiment are quite nonlinear. In addition, there are surely preexisting nonideal phase space structures in the beam which are not included in our models. Such phase space artifacts may arise from temporal structure in the drive laser pulse and nonuniform emission from the photocathode. These effects provide an initial filamentary structure to the phase space, which can be amplified by the mechanisms discussed above.

The study of such nonideal beam effects must be pursued further. Two comments are relevant here: first, nonideal beam effects may also help to resolve the differences between data and simulations in other compression experiments. Second, we note that, in all codes we employed, significant $\Delta\varepsilon_{n,x}$ was observed after the chicane, where the compressed beam distribution relaxes, converting nonlinear field energy (density nonuniformities) to emittance (phase space nonuniformities). The emittance compensation process essentially images spatial nonuniformities from the cathode to the chicane entrance, thus maximizing the nonlinear field energy there. This conversion process maximizes $\Delta\varepsilon_{n,x}$ and the associated phase space distortion after one-quarter of a beam-plasma oscillation [27,28] ($\lambda_p = \sqrt{\pi\gamma^3/r_e n_b}$), where n_b is the beam density and r_e is the classical electron radius. For this experiment, the length between the chicane exit and the slits was in fact very close to $\lambda_p/4$, especially for cases where $\sigma_{x,0}$ was small.

The authors thank C. Joshi, C. Pellegrini, R. Agustsson, S. Boucher, C. Clayton, T. Holden, M. Loh, H. Suk, S. Telfer, and A. Tremaine for their support and contributions. This work was performed with support from U.S. Department of Energy Grant No. DE-FG03-92ER40693.

[1] International Study Group, Technical Report No. SLAC-R-559, Stanford Linear Accelerator Center, 2000.
[2] J. B. Rosenzweig *et al.*, IEEE Trans. Plasma Sci. **24**, 409 (1996).
[3] The LCLS Design Study Group, Technical Report No. SLAC-R-0521, Stanford Linear Accelerator Center, 1998.
[4] M. Reiser, *Theory and Design of Charged Particle Beams* (Wiley, New York, 1994).
[5] B. E. Carlsten, Nucl. Instrum. Methods Phys. Res., Sect. A **285**, 313 (1989).
[6] L. Serafini and J. B. Rosenzweig, Phys. Rev. E **55**, 7565 (1997).
[7] M. James *et al.*, IEEE Trans. Nucl. Sci. **NS-30**, 2992 (1983).
[8] S. Heifets *et al.*, Phys. Rev. ST Accel. Beams **5**, 064401 (2002).
[9] H. Braun *et al.*, Phys. Rev. Lett. **84**, 658 (2000).
[10] H. Braun *et al.*, Phys. Rev. ST Accel. Beams **3**, 124402 (2000).
[11] M. Dohlus *et al.*, in *Proceedings of the 1999 Particle Accelerator Conference* (IEEE, New York, 1999), p. 1650.
[12] ICFA Beam Dynamics mini workshop (2002), see http://www.desy.de/csr/csr_workshop_2002/csr_workshop_2002_index.html.
[13] G. P. LeSage *et al.*, in *Advanced Accelerator Concepts: Ninth Workshop*, edited by P. L. Colestock and S. Kelley, AIP Conf. Proc. No. 569 (AIP, New York, 2001).
[14] J. B. Rosenzweig *et al.*, Nucl. Instrum. Methods Phys. Res., Sect. A **410**, 437 (1998).
[15] D. T. Palmer, Ph.D. thesis, Stanford University, 1998.
[16] R. Zhang *et al.*, in *1995 Particle Accelerator Conference* (IEEE, New York, 1995), p. 1102.
[17] K. R. Crandall and L. Young, Technical Report No. LA-UR-90-1766, Los Alamos National Laboratory, 1990.
[18] U. Happek, A. J. Sievers, and E. B. Blum, Phys. Rev. Lett. **67**, 2962 (1991).
[19] A. Murokh *et al.*, Nucl. Instrum. Methods Phys. Res., Sect. A **410**, 452 (1998).
[20] C. Lejeune and J. Aubert, in *Advances in Electronics and Electron Physics* (Academic, New York, 1980), Suppl. 13A, p. 159.
[21] S. G. Anderson *et al.*, Phys. Rev. ST Accel. Beams **5**, 014201 (2002).
[22] S. G. Anderson, Ph.D. thesis, University of California, Los Angeles, 2002.
[23] F. Ciocci *et al.*, Nucl. Instrum. Methods Phys. Res., Sect. A **393**, 434 (1997).
[24] L. Young and J. Billen, Technical Report No. LA-UR-96-1835, Los Alamos National Laboratory, 1996.
[25] B. E. Carlsten and T. O. Raubenheimer, Phys. Rev. E **51**, 1453 (1995).
[26] M. Borland, Technical Report No. LS-287, Argonne National Laboratory Advanced Photon Source, 2000.
[27] O. A. Anderson, Part. Accel. **21**, 197 (1987).
[28] S. G. Anderson and J. B. Rosenzweig, Phys. Rev. ST Accel. Beams **3**, 094201 (2000).